Biophysical Journal
Article

Biophysical Society

Spatial Fluctuations at Vertices of Epithelial Layers: Quantification of Regulation by Rho Pathway

Étienne Fodor,[1,2] Vishwajeet Mehandia,[3,4,5] Jordi Comelles,[3,4] Raghavan Thiagarajan,[3,4] Nir S. Gov,[6] Paolo Visco,[2] Frédéric van Wijland,[2] and Daniel Riveline[3,4,*]

[1]DAMTP, Centre for Mathematical Sciences, University of Cambridge, Cambridge, United Kingdom; [2]Laboratoire Matière et Systèmes Complexes, UMR 7057 CNRS/P7, Université Paris Diderot, Paris cedex 13, France; [3]Laboratory of Cell Physics, ISIS/IGBMC, Université de Strasbourg and CNRS (UMR 7006), Strasbourg, France; [4]Development and Stem Cells Program, IGBMC, CNRS (UMR 7104), INSERM (U964), Université de Strasbourg, Illkirch, France; [5]School of Mechanical, Materials and Energy Engineering, Indian Institute of Technology, Ropar, India; and [6]Department of Chemical Physics, Weizmann Institute of Science, Rehovot, Israel

ABSTRACT In living matter, shape fluctuations induced by acto-myosin are usually studied in vitro via reconstituted gels, whose properties are controlled by changing the concentrations of actin, myosin, and cross-linkers. Such an approach deliberately avoids consideration of the complexity of biochemical signaling inherent to living systems. Acto-myosin activity inside living cells is mainly regulated by the Rho signaling pathway, which is composed of multiple layers of coupled activators and inhibitors. Here, we investigate how such a pathway controls the dynamics of confluent epithelial tissues by tracking the displacements of the junction points between cells. Using a phenomenological model to analyze the vertex fluctuations, we rationalize the effects of different Rho signaling targets on the emergent tissue activity by quantifying the effective diffusion coefficient, and the persistence time and length of the fluctuations. Our results reveal an unanticipated correlation between layers of activation/inhibition and spatial fluctuations within tissues. Overall, this work connects regulation via biochemical signaling with mesoscopic spatial fluctuations, with potential application to the study of structural rearrangements in epithelial tissues.

INTRODUCTION

Changes in shapes of cells and tissues are mediated by the acto-myosin cytoskeleton. To reproduce the dynamics of this network, small systems made of actin filaments, myosin motors, and cross-linkers are synthetized in vitro (1–5). The mechanics and dynamics of such active gels are controlled by varying the concentration of their various components. The activity of each component is monitored by adding some inhibitor drugs and/or by tuning the ATP concentration of the system. Recent experimental evidence has shown the relevance of this approach to the investigation of the role of motors and cross-linkers in the emerging properties of the network (2,6). These studies are based on tracking the motion of tracers injected in active gels; analyzing the spontaneous fluctuations of such tracers enables one to extract information about the activity of internal motors.

In multicellular systems, such as tissues of developing embryos, acto-myosin drives morphogenesis: dramatic rearrangements leading to the formation of distinct organs (7,8). This remodeling is mainly under the control of intracellular activity, which powers spatial fluctuations (9), and intercellular interactions mediated by adhesion between neighboring cells (10,11). In contrast to synthetic gels, the internal regulation of the cellular acto-myosin activity is more complex in vivo. Therefore, extending the in vitro approach, based on externally controlling the activity of each specific component, to in vivo situations requires new strategies.

The Rho signaling pathway is known to regulate acto-myosin activity in living cells (12). It also controls cell-cell junctions (13) and the elasticity of stress fibers (14). Such a pathway can be viewed as a series of activators and inhibitors installing a hierarchy of potential targets (15,16). Activations and inhibitions controlled by each target are such that anticipating their net effects on the tissue fluctuations, powered by acto-myosin activity, remains a challenge (17,18). In that respect, the inherent complexity of internal activity in vivo calls for new experiments and quantitative analysis to bridge the biochemical signaling of the Rho pathway with the emerging tissue dynamics.

In this study, we explore the regulation of active fluctuations by the Rho pathway in epithelial monolayers.

Submitted June 9, 2017, and accepted for publication December 20, 2017.

*Correspondence: riveline@unistra.fr

Étienne Fodor and Vishwajeet Mehandia contributed equally to this work.

Editor: Jennifer Curtis.

https://doi.org/10.1016/j.bpj.2017.12.026

We measure these fluctuations by tracking tricellular junctions or vertices over time. In contrast to active gels, our analysis of internal fluctuations does not require the injection of external tracers. Based on a phenomenological model, we quantify key parameters of junction activity: their effective diffusion coefficient, as well as the persistence time and length of spatial fluctuations. We report modifications of these parameters for various targets along the signaling pathway. These results support the idea that, for the inhibitions that we have considered, the active fluctuations of the vertices are reduced when the Rho pathway is inhibited downstream.

MATERIALS AND METHODS

Experiments were performed with Madin Darby Canine Kidney (MDCK) II cells stably expressing E-cadherin Green Fluorescent Protein (Nelson Lab). We cultured cells in Dulbecco's Modified Eagle Medium containing 10% fetal calf serum and antibiotics. We replated them on 25 mm diameter glass cover slips (CS) for live cell imaging. When the cell monolayer covered 70% of the CS area, we firmly placed the sample at the bottom of a custom made metallic holder. For acquisition, we changed the medium to L15, 10% fetal calf serum, and antibiotics. We use the following inhibitors from myosin up to Rho at optimal concentrations following the manufacturer's recommendations: inhibition of acto-myosin by ML-7 (10 μM; Sigma-Aldrich, St. Louis, MO), inhibition of Rho kinase (ROCK) by Y-27632 (10 μM; Sigma-Aldrich), and inhibition of Rho by C3 Transferase (Cytoskeleton, 0.04 μM). Note that the use of blebbistatin to directly inhibit myosins yielded some detrimental effects, leading us to use ML-7 instead.

For observation, we use a motorized inverted microscope (Nikon Eclipse Ti), equipped with a 12 bit charge-coupled device camera (Photometric CoolSNAP HQ2). The setup was temperature controlled at 37°C (Life Imaging Services, Basel, Switzerland). We checked that no drift appeared during 24 h of live imaging after 2 h stabilization with fluorescent beads (4 μm; TetraSpeck, Invitrogen Molecular Probes) grafted on the CS surface. We took pictures of the monolayer every 5 min during the next 8 h with multiple z-stacks 1 μm apart. They spanned 3 μm depth of the cell monolayer. We then merged the z-stacks into one image by using the maximum intensity projection, and extracted vertex positions from the sequence of merged images by manually clicking in each frame as long as they were visible. The procedure was also validated in its precision through automated detection. For each condition, we checked that the average cell area was always about 180 ± 15 μm^2, and we considered more than 20 vertices for at least three biological repeats.

RESULTS

Vertex tracking and inhibitors in the Rho pathway

We use MDCK cells stably transfected with E-cadherin fused with Green Fluorescent Protein as a paradigm for epithelial tissues dynamics (19). This allows us to study live cells, although they are interacting with each other. We seek to identify spatial points primarily involved in tissue transformations. The meeting points between three cells are involved in exchanges between neighboring cells, thus serving as a hallmark of tissue dynamics (11,20). Some specific proteins, such as tricellulin, are known to accumulate at this point in cell culture. Besides, vertices that exhibit accumulation of proteins at these specific points have also attracted the attention of developmental biologists (21).

Vertex dynamics are driven both by thermal fluctuations and by active fluctuations powered by some internal nonequilibrium processes such as motor-induced forces, actin polymerization, and cell-cell adhesion. The myosin-II motors are localized in dense contractile units present in the apical surface of the tissue (22,23) Fig. 1, *a–c*. The active forces lead to large displacements of the vertices distinct from the thermal fluctuations of smaller amplitude. We focus here on large displacements that do not lead to any topological transitions in the tissue Fig. 1, *d* and *e*. The Rho signaling pathway controls the acto-myosin activity inside cells, namely the forces induced by myosin and/or by actin polymerization (see Fig. 9 in (16)). In this study, we focused on the downstream targets that affect myosin to establish the principles for the validity and relevance of our framework. Upstream and downstream targets install a hierarchy in the activation of myosin. We specifically inhibited the following targets: Rho, ROCK, and myosin-II Fig. 1 *f*. Each inhibitor is specific to its target and incubation was conducted at the optimal concentrations for its inhibition. We used standard concentration values already utilized in other cell biology studies for many cell types including MDCK (24–27). Altogether, we probed four conditions on the same system by considering untreated cells as a control.

To demonstrate that the chosen inhibitors and their concentrations specifically act on the contractile state of cells, we investigated their effect on both architecture and contractile forces within tissues by measuring the single cell area and myosin cluster area in each condition. The distribution of single cell area is not strongly affected in the myosin-II inhibitor case compared with control, as apparent from the mean value in Fig. 1 *g*. The distribution gets modified in the ROCK and Rho inhibitor cases, with mean values being slightly reduced and increased, respectively. In contrast, the polygonicity distribution remains approximately the same for all conditions at different times, supporting the notion that tissue architecture is barely affected by external inhibitors (see Fig. S1).

Myosin clusters have been shown to be relevant read-outs to assess the contractile state of cells (28,29). Along this line, measurements of cluster characteristics are informative. In our case, the mean density value of myosin clusters for the control is larger than in the inhibited cases (see Fig. S2), suggesting a decrease in force generation for the same level of myosin per cell. In addition, the area of each myosin cluster is smaller in the control than in other conditions Fig. 1 *h*. Besides, this area increases with increasing distance downstream of the Rho pathway inhibition, suggesting a relaxation of the myosin pool in the apical side, consistent with the notion that myosin-induced forces are reduced. Altogether, our analysis of clusters confirms that we are acting on the contractile state of cells. Since inhibitors are specific and used at their optimal

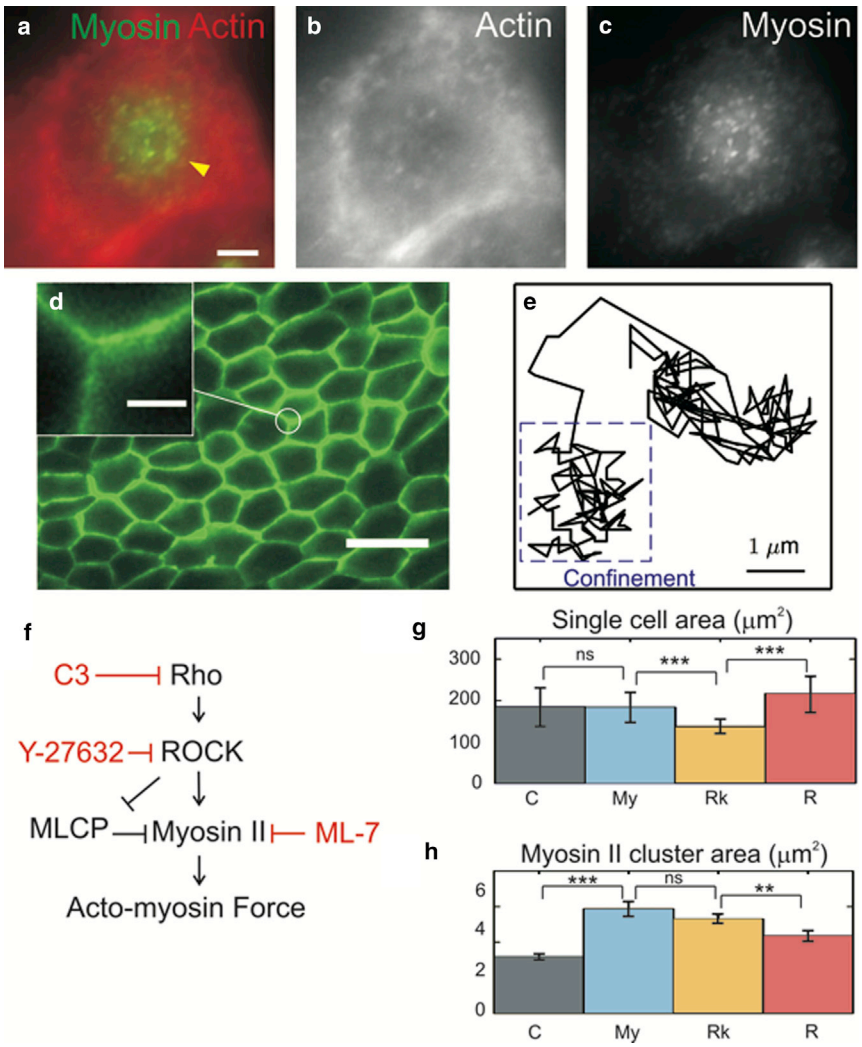

FIGURE 1 Study of vertex fluctuations. (*a*) Actin (*red*) and myosin (*green*) structures at the apical surface of a MDCK cell. Scale bar, 3 μm. The myosin is concentrated in dense contractile units (*yellow arrow*) referred to as myosin clusters. (*b*) Actin structure alone. (*c*) Myosin structure alone. (*d*) MDCK cell monolayer shown by Green Fluorescent Protein E-cadherin. Scale bar, 30 μm. (*Inset*) The meeting points between three cells are identified as the privileged point for our analysis. Scale bar, 4 μm. (*e*) Extraction of a typical transition between two locally stable positions in a vertex trajectory (total time 8 h). (*f*) Simplified diagram of the Rho pathway installing an order relation in myosin activation, as presented in (16); the specific inhibitors and their targets are shown in red. (*g*) Area of individual cells in each condition. C, Control; My, Myosin inhibitor; Rk, ROCK inhibitor; and R, Rho inhibitor. Number of experiments × number of cells = C: 4 × 235; My: 4 × 246; Rk: 3 × 249; R: 3 × 148. (*h*) Area of myosin clusters. Number of experiments × number of clusters = C: 2 × 312; My: 2 × 186; Rk: 2 × 197; R: 2 × 257. Statistical analysis with one-way ANOVA test: ns (nonsignificant),$p > 0.05$, *$p < 0.05$, **$p < 0.01$, and ***$p < 0.001$ (see the Supporting Material). To see this figure in color, go online.

concentrations, these measurements support the validity of our experimental approach.

Statistics of vertex displacement: inhibitors affect spatial fluctuations

Our goal is to investigate how the emergent fluctuations of the tissue are regulated by the Rho pathway. To this aim, we first demonstrated that the inhibitors in the pathway affect these fluctuations by extracting the statistics of displacements from the vertex trajectories. This allowed us to assess the existence of a direct link between biochemical signaling and mechanical fluctuations. In our analysis, we considered neither spatial inhomogeneities nor topological transitions that occur in the tissues. In that respect, we measured vertex trajectories in the absence of neighboring cell division by tracking them as long as they were visible until a maximum of 8 h.

We computed the projected one-dimensional mean square displacement (MSD) within the four different conditions Fig. 2 *a*. For each condition, the short time MSD exhibited a power-law behavior with exponent close to 0.7 over about one decade. Interestingly, a subdiffusive behavior was reported for the dynamics of vertices in the endoplasmic reticulum (30). The large time MSD depends on conditions and exhibits a behavior that, for simplicity, we have characterized by a power-law. The corresponding exponent was typically > 1, except for the myosin inhibitor where it was smaller. The crossover between the two regimes appeared between 20 and 60 min. Fluctuations were reduced in the myosin-inhibited case, which had the lowest MSD, and they were enhanced for the Rho inhibitor, where the long time MSD was the largest. We also explored the full statistics of vertex displacement by measuring the probability distribution function (PDF) for each condition, as shown in Fig. 2, *b–e*. At short time the PDF is Gaussian, although it exhibits broader tails at long time. These tails reveal large displacements of the vertex, and have already been observed for tracer particles in active gels (31) and living cells (32–36). They are more pronounced in the Rho inhibitor case as a signature of larger fluctuations, possibly due to directed motion events.

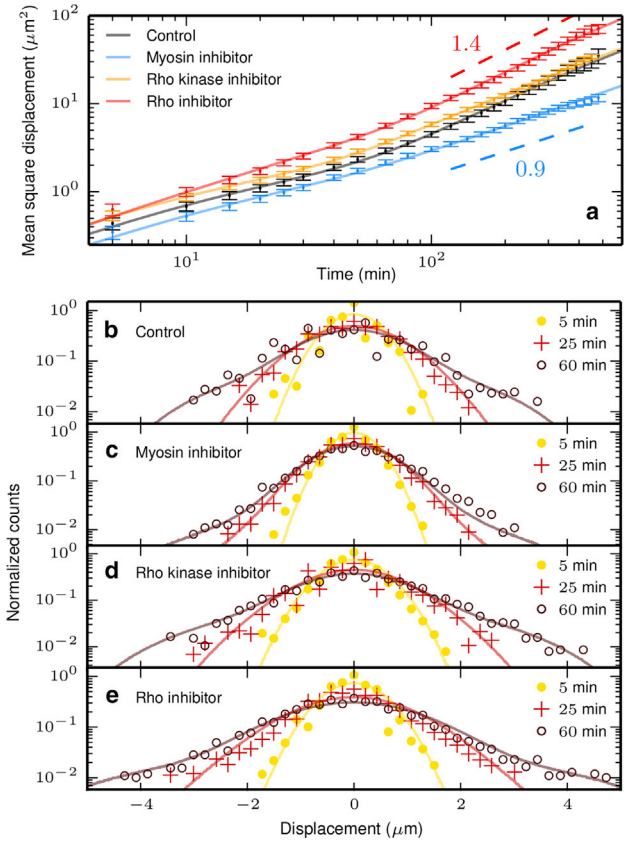

FIGURE 2 Statistics of vertex displacement. (*a*) Mean square displacement as a function of time in four conditions: control (*black*), myosin inhibitor (*blue*), ROCK inhibitor (*orange*), and Rho inhibitor (*red*). The corresponding best-fitting curves are shown as solid lines. The blue and red dashed lines report the large time behaviors. (*b–e*) Distribution of displacement for the four conditions at three times: 5 (*yellow filled circles*), 25 (*red crosses*), and 60 min (*unfilled circles*). Exponential tails appear at long times as a consequence of directed motion events in vertex dynamics. Results of simulated dynamics are in solid lines. To see this figure in color, go online.

Phenomenological model of vertex dynamics: transient confinements and large displacements

To quantitatively discriminate between the effects of the different inhibitors, we analyzed our measurements with a nonequilibrium model previously introduced to describe tracer fluctuations inside living cells (36). This model is not aimed at describing any specific process that produces the active fluctuations, but rather formulates a general framework that allows one to quantify nonequilibrium forces and fluctuations. We regard the vertex as a virtual particle in which dynamics are prescribed by two coupled equations: 1) an equilibrium diffusion of the vertex in a cage, modeled as an harmonic potential of stiffness k (the displacement is driven by a Gaussian white noise of variance $2\gamma k_{\mathrm{B}}T$ with a drag force of coefficient γ), and 2) a non-Gaussian colored diffusion equation for the center of the cage, mimicking nonequilibrium activity as a run-and-tumble dynamic. Inspired by the large ballistic-like displacements that we observe in experimental trajectories, we modeled this active noise as a two-state Poisson process: the cage has a constant velocity v in a random, uniformly sampled two-dimensional direction during a random persistence time of average τ, and it remains fixed during a random quiescence time of mean τ_0. We understand the confinement as an elastic mechanical stress resulting from cells surrounding each vertex, and the nonequilibrium motion of the cage as an active stress. The effect of this active stress is to reorganize the structure of the monolayer, and therefore to spatially redistribute the elastic mechanical stress.

In the absence of activity, this model predicts a short time diffusion, and then a large time plateau expressing the elastic confinement. Such dynamics are entirely under the control of equilibrium thermal fluctuations. In an active system, nonequilibrium processes enhance vertex displacement via the cage motion, yielding a free diffusion of the vertex with coefficient $D_{\mathrm{A}} = (v\tau)^2/[2(\tau+\tau_0)]$. The large time dynamics are fully determined by the active parameters $\{v,\tau,\tau_0\}$, whereas thermal fluctuations control the short times *via* $\{k,\gamma,T\}$. A subdiffusive transient regime appears between the two diffusions as a crossover toward a plateau, and a superdiffusive regime can also precede the large time diffusion as a signature of the ballistic motion involved in the active noise. In such a case, thermal effects are negligible at times larger than $\tau_{\mathrm{c}} = \sqrt{\tau k_{\mathrm{B}}T/(kD_{\mathrm{A}})}$, a timescale quantifying the transition from the short time equilibrium-like dynamics to the large time active diffusion. Simulated trajectories exhibit clusters of similar size accounting for the transient confinement of the vertex. Occasionally, large displacements of order $v\tau$ appear. The vertices do not only fluctuate around a local equilibrium position, but also undergo rapid directed jumps (compare Figs. 1 *e* and 3 *a*).

In contrast to previous works that describe the many-body dynamics of cells in the tissue in a more complete framework (37–39), we do not explicitly account for interactions between neighboring vertices. As a result of such interactions, the cells experience an intermittent dynamic alternating between fluctuations of small amplitude and rapid large displacements. As in glassy systems, the jumps appear through collective rearranging regions (40), thus contributing to the non-Gaussian fluctuations experienced by the vertices. Even though non-Gaussian fluctuations are present independently of topological transitions, the existence of a quantitative connection between collective rearrangements and such transitions is still an open question (41). Our approach consists in reducing the dynamics of a large number of interacting vertices into the dynamics of a single vertex embedded in an effective background, which describes the mean-field effect of the surrounding system. Within our model, interactions are embodied by both the elastic confinement and the active source of fluctuations leading to large displacements. We argue below that our phenomenological approach is sufficient to capture the vertex

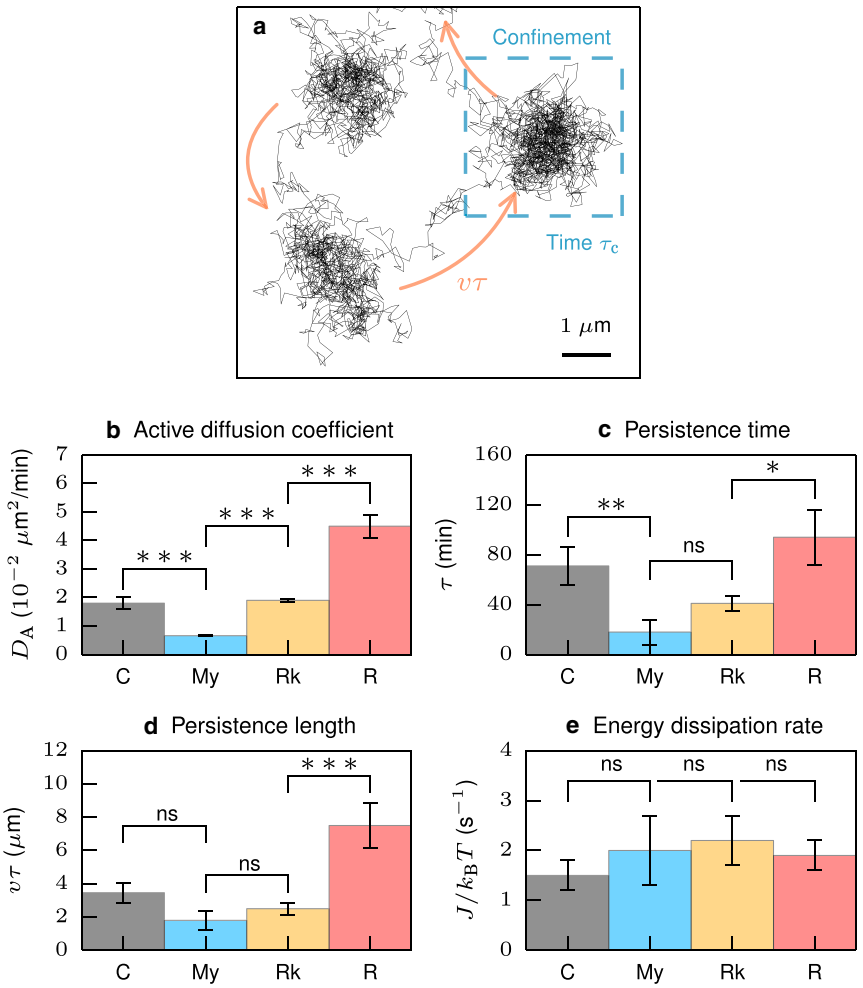

FIGURE 3 Active parameters of vertex fluctuations. (*a*) Typical trajectory obtained from simulations of the vertex dynamics in control conditions. Scale bar, 1 μm. Isotropic "blobs" reveal equilibrium-like transient confinement during a typical time τ_c (*dashed blue box*), and large displacements of order $v\tau$ occur due to nonequilibrium activity (*orange arrows*). (*b*) Best fit values of the active diffusion coefficient, (*c*) the persistence time and the typical confinement time, (*d*) the persistence length, and (*e*) the energy dissipation rate. Statistical analysis with Student's *t*-test: ns (nonsignificant), $p > 0.05$, *$p < 0.05$, **$p < 0.01$, and ***$p < 0.001$, (see the Supporting Material). To see this figure in color, go online.

dynamics, since it provides a framework to decipher the effects of Rho pathway inhibition on these dynamics.

Order relation in the active diffusion coefficient and the persistence time

When we fit the MSD data with our analytic prediction to estimate the parameters characterizing nonequilibrium activity, our fits convincingly capture the transition from subdiffusive to superdiffusive-like behaviors Fig. 2 *a*. Within our model, these behaviors correspond to crossover regimes between the short and large time diffusion. We extract from the best fits a single set of passive and active parameters for each condition. Our estimate for τ_c can be compared with timescales quantifying the transition from the elastic to fluid-like behavior of the material (see Table S1), which is of the same order as the Maxwell time reported in three-dimensional cell aggregates, i.e., ~30–40 min (9,42–44). We report clear quantitative variations of both the active diffusion coefficient D_A and the persistence time τ for all conditions Fig. 3, *b* and *c*. This suggests that our model, based on separating purely active fluctuations from equilibrium thermal ones, is a reliable framework to capture the effects of our inhibitors on tissue dynamics. Note that passive parameters, such as the relaxation time scale $\tau_r = \gamma/k$ reported in Table S1 (see the Supporting Material), also have different values between the conditions. This reflects the effects of inhibitors on tissue mechanics, showing that inhibitors also affect the characteristics of passive fluctuations. In this respect, D_A and τ are the parameters that characterize only the active contribution to vertex fluctuations, which is the main focus of our study.

Strikingly, D_A and τ are larger for Rho inhibitor than for ROCK inhibitor and for direct myosin inhibition Fig. 3, *b* and *c*. The more upstream the inhibition along the pathway, the larger the amplitude of fluctuations and the more persistent the ensuing displacement. The myosin inhibition leads to the smallest D_A and τ values, suggesting that the mesoscopic activity of vertices is strongly affected. The ROCK target directly activates the myosin, but it also inhibits the myosin light chain phosphatase, which in turn inhibits the myosin. Therefore, the result of ROCK inhibition on myosin cannot be anticipated a priori. Our analysis shows that the activity of vertices is less affected than for the myosin inhibitor

case: the corresponding value of D_A for the ROCK inhibitor is close to the one for the control, which suggests a compensation between the activation and deactivation of myosin.

Order relation confirmed by persistence lengths

To gain further insight into the active component of the dynamics, we compare the displacement PDF extracted from the simulated trajectories of vertex dynamics with experimental distributions. The distribution at short time is Gaussian and entirely controlled by the passive parameters: the simulations with or without active fluctuations, where we use passive parameters estimated from fits of MSD data, give the same results at short times (see yellow curves in Fig. 2, *b–e*). Including the active component for the dynamics leaves us with one remaining free parameter: the average persistence length $v\tau$ of large displacements. The short time Gaussian remains unchanged, whereas exponential tails develop at large times in the simulated PDF. The tails are more pronounced as time increases, whereas the central Gaussian part barely changes. We adjust the $v\tau$ value by matching the tails appearing in numerical results and experimental data.

The simulated PDFs compare very well with experiments at large times, showing that our simulations reproduce the evolution of experimental distributions at all times Fig. 2, *b–e*. This is one of the main successes of our analysis: the phenomenological model on which the quantification of internal activity relies is able to capture the strong non-Gaussian tails of the distribution with only one free parameter. This supports the underlying picture that vertex dynamics essentially alternate between transient confinement and directed motions. The order of magnitude of the extracted mean persistence length $v\tau$ is consistent with our measurements Fig. 3 *d*. We report again the same order relationship within the Rho pathway, i.e., an increase of $v\tau$ from myosin inhibitor to ROCK inhibitor, and from ROCK inhibitor to Rho inhibitor, as a signature of enhanced directed motion.

Dissipation is constant for all inhibitors

A major asset of our model is that it allows us to predict the mean rate of energy dissipated by the vertex dynamics in its surrounding environment. It is defined as the difference between the power injected by the fluctuating thermal force and the one that the moving vertex dissipates *via* the drag force: $J = \langle \dot{x}(\gamma\dot{x} - \sqrt{2\gamma k_B T}\,\xi)\rangle$, where $\dot{x}$ is the vertex velocity and ξ is a zero-mean Gaussian white noise (45,46). It vanishes for systems in a thermodynamic equilibrium state. The active nonequilibrium fluctuations lead to a nonzero dissipation rate: $J = kD_A/(1 + \tau/\tau_r)$ (47). This rate of dissipated energy reflects the excess power injected by nonequilibrium internal activity driving the large displacements of vertices.

When computing the dissipation rate in the four conditions, it appears as approximately constant (Fig. 3 *e*), in contrast to the order relation found for active parameters (Fig. 3, *b–d*). This supports the notion that the same amount of energy is dissipated by the vertex large displacements, though the features of such displacements differ between conditions. Given that J depends both on parameters of active fluctuations $\{D_A, \tau\}$ and on parameters of passive mechanics $\{\gamma, k\}$, our result suggests that there may be an underlying coupling between mechanical properties of the tissue and its nonequilibrium fluctuations. A possible interpretation is that the nonequilibrium processes at the origin of active fluctuations, such as forces induced by myosin and by actin polymerization, might also affect the tissue mechanics in such a way that the dissipation rate remains unchanged over all the conditions. In that respect, we observe that the relaxation time τ_r is increased for the case of the Rho inhibitor case with respect to others (see Table S1), as also observed for the persistence time τ (Fig. 3 *c*).

DISCUSSION

The parameters of vertex fluctuations reveal a correlation between the Rho pathway hierarchy and the junction active fluctuations: the higher up the Rho pathway the inhibition, the lower the effect on the decreasing fluctuations of the vertices. Such a relationship highlights the usefulness of our methodology for quantitatively probing how signaling pathways control emergent fluctuations. In that respect, our approach bridges biochemical signaling pathways with mechanical fluctuations in vivo. It could be used to quantitatively characterize the effect of other inhibitions acting on different signaling pathways on fluctuations.

Our analysis is based on a phenomenological model, which deliberately avoids a detailed description of the many processes operating at the subcellular scale. It is also distinct from other models that consider explicit interactions between neighboring cells. In that respect, our results rely neither on the microscopic details of activity-induced forces nor on the form of interactions within the tissue. Rather, we postulate an effective vertex dynamic by explicitly distinguishing thermal and active fluctuations. As a result, any underlying mechanism that could rationalize the relationship between pathway inhibition and mechanical fluctuation is out of the scope of our approach. Yet, the relationship between biochemical signaling and active fluctuations that we have quantified in tissues could help future studies to understand the precise relationship between subcellular cytoskeleton dynamics and emergent vertex fluctuations. In that respect, a possible extension of the model could involve considering more complex activation/inhibition in the Rho pathway and their connection with contractile forces in the cell (17,18).

To test the robustness of our model, one could measure the response of vertices to an external perturbation (48).

The intracellular mechanics are viscoelastic in a large variety of living systems. Our phenomenological model has already been extended to account for a complex rheology (49). It would be interesting to determine whether the relationship between fluctuations and pathway inhibition is similar when viscoelastic effects are included. Moreover, applying an external potential to confine a vertex, one could extract work from the vertex fluctuations by varying the potential parameters in time. Our framework allows one to predict the details of the extracted work as a function of the active fluctuation characteristics (47). Confronting such predictions with experimental results would provide another test for the validity of our approach.

Responses in living systems are not related to spontaneous fluctuations, in contrast to equilibrium, where such a relationship is given by the fluctuation-dissipation theorem (FDT). Therefore, by comparing responses with spontaneous fluctuations of tissues, one could quantify the departure from the FDT, namely the deviation of the dynamics from equilibrium. Moreover, recent progress in nonequilibrium statistical mechanics has shed light on the direct relationship between the rate of energy dissipated by the internal nonequilibrium processes and the violation of the FDT (50). This has already led to access to the dissipation rate in some biological contexts (49,51). In that respect, comparing responses and fluctuations will allow the proposition of an alternative method for the quantification of dissipation rates in epithelial tissues.

The Rho pathway is conserved across species, suggesting that the regulation of activity in epithelial monolayers may share common pathways in a large variety of tissues and organisms (12). Our approach, based on a quantitative analysis of vertex fluctuations, could serve as, to our knowledge, a novel framework to decipher the complex regulation of spatial fluctuations by the Rho pathway in other model systems. In that respect, it could be used to analyze vertex fluctuations in developing embryos, such as in *Drosophila* or in *Caenorhabditis elegans*, where internal reorganization is driven by spontaneous topological transition (7,8).

SUPPORTING MATERIAL

Supporting Materials and Methods, two figures, and three tables are available at http://www.biophysj.org/biophysj/supplemental/S0006-3495(17)35130-5.

AUTHOR CONTRIBUTIONS

V.M., J.C., R.T., and D.R. designed and performed the experiments. É.F., N.S.G., P.V., and F.v.W. designed the model. All authors contributed to analyzing the data and writing the manuscript.

ACKNOWLEDGMENTS

We thank F. Graner for helpful discussions, J. W. Nelson for sending the MDCK cell lines, N. Maggartou for extraction of data, and laboratory members for discussions. This work was supported by the Centre National de la Recherche Scientifique, Fondation pour la Recherche en Chimie, and University of Strasbourg. N.S.G. is the incumbent of the Lee and William Abramowitz Professorial Chair of Biophysics.

REFERENCES

1. Backouche, F., L. Haviv, …, A. Bernheim-Groswasser. 2006. Active gels: dynamics of patterning and self-organization. *Phys. Biol.* 3:264–273.
2. Soares e Silva, M., B. Stuhrmann, …, G. H. Koenderink. 2014. Time-resolved microrheology of actively remodeling actomyosin networks. *New J. Phys.* 16:075010.
3. Blanchoin, L., R. Boujemaa-Paterski, …, J. Plastino. 2014. Actin dynamics, architecture, and mechanics in cell motility. *Physiol. Rev.* 94:235–263.
4. Murrell, M., P. W. Oakes, …, M. L. Gardel. 2015. Forcing cells into shape: the mechanics of actomyosin contractility. *Nat. Rev. Mol. Cell Biol.* 16:486–498.
5. Schuppler, M., F. C. Keber, …, A. R. Bausch. 2016. Boundaries steer the contraction of active gels. *Nat. Commun.* 7:13120.
6. Soares e Silva, M., M. Depken, …, G. H. Koenderink. 2011. Active multistage coarsening of actin networks driven by myosin motors. *Proc. Natl. Acad. Sci. USA.* 108:9408–9413.
7. Rauzi, M., P. Verant, …, P.-F. Lenne. 2008. Nature and anisotropy of cortical forces orienting Drosophila tissue morphogenesis. *Nat. Cell Biol.* 10:1401–1410.
8. Guillot, C., and T. Lecuit. 2013. Mechanics of epithelial tissue homeostasis and morphogenesis. *Science.* 340:1185–1189.
9. Marmottant, P., A. Mgharbel, …, H. Delanoë-Ayari. 2009. The role of fluctuations and stress on the effective viscosity of cell aggregates. *Proc. Natl. Acad. Sci. USA.* 106:17271–17275.
10. Cavey, M., M. Rauzi, …, T. Lecuit. 2008. A two-tiered mechanism for stabilization and immobilization of E-cadherin. *Nature.* 453:751–756.
11. Bardet, P.-L., B. Guirao, …, Y. Bellaïche. 2013. PTEN controls junction lengthening and stability during cell rearrangement in epithelial tissue. *Dev. Cell.* 25:534–546.
12. Etienne-Manneville, S., and A. Hall. 2002. Rho GTPases in cell biology. *Nature.* 420:629–635.
13. Reyes, C. C., M. Jin, …, A. L. Miller. 2014. Anillin regulates cell-cell junction integrity by organizing junctional accumulation of Rho-GTP and actomyosin. *Curr. Biol.* 24:1263–1270.
14. Oakes, P. W., E. Wagner, …, M. L. Gardel. 2017. Optogenetic control of RhoA reveals zyxin-mediated elasticity of stress fibres. *Nat. Commun.* 8:15817.
15. Gibson, M. C., A. B. Patel, …, N. Perrimon. 2006. The emergence of geometric order in proliferating metazoan epithelia. *Nature.* 442:1038–1041.
16. Riveline, D., E. Zamir, …, A. D. Bershadsky. 2001. Focal contacts as mechanosensors: externally applied local mechanical force induces growth of focal contacts by an mDia1-dependent and ROCK-independent mechanism. *J. Cell Biol.* 153:1175–1186.
17. Besser, A., and U. S. Schwarz. 2007. Coupling biochemistry and mechanics in cell adhesion: a model for inhomogeneous stress fiber contraction. *New J. Phys.* 9:425.
18. Bement, W. M., M. Leda, …, G. von Dassow. 2015. Activator-inhibitor coupling between Rho signalling and actin assembly makes the cell cortex an excitable medium. *Nat. Cell Biol.* 17:1471–1483.
19. Adams, C. L., Y. T. Chen, …, W. J. Nelson. 1998. Mechanisms of epithelial cell-cell adhesion and cell compaction revealed by high-resolution tracking of E-cadherin-green fluorescent protein. *J. Cell Biol.* 142:1105–1119.

20. Salomon, J., C. Gaston, …, D. Delacour. 2017. Contractile forces at tricellular contacts modulate epithelial organization and monolayer integrity. *Nat. Commun.* 8:13998.

21. Lye, C. M., H. W. Naylor, and B. Sanson. 2014. Subcellular localisations of the CPTI collection of YFP-tagged proteins in *Drosophila* embryos. *Development.* 141:4006–4017.

22. Rauzi, M., P.-F. Lenne, and T. Lecuit. 2010. Planar polarized actomyosin contractile flows control epithelial junction remodelling. *Nature.* 468:1110–1114.

23. Klingner, C., A. V. Cherian, …, R. Wedlich-Soldner. 2014. Isotropic actomyosin dynamics promote organization of the apical cell cortex in epithelial cells. *J. Cell Biol.* 207:107–121.

24. Jin, Y., S. J. Atkinson, …, P. J. Gallagher. 2001. Myosin ii light chain phosphorylation regulates membrane localization and apoptotic signaling of tumor necrosis factor receptor-1. *J. Biol. Chem.* 276:30342–30349.

25. Reffay, M., M. C. Parrini, …, P. Silberzan. 2014. Interplay of RhoA and mechanical forces in collective cell migration driven by leader cells. *Nat. Cell Biol.* 16:217–223.

26. Sorce, B., C. Escobedo, …, D. J. Müller. 2015. Mitotic cells contract actomyosin cortex and generate pressure to round against or escape epithelial confinement. *Nat. Commun.* 6:8872.

27. Imai, M., K. Furusawa, …, H. Haga. 2015. Three-dimensional morphogenesis of MDCK cells induced by cellular contractile forces on a viscous substrate. *Sci. Rep.* 5:14208.

28. Munjal, A., and T. Lecuit. 2014. Actomyosin networks and tissue morphogenesis. *Development.* 141:1789–1793.

29. Wollrab, V., R. Thiagarajan, …, D. Riveline. 2016. Still and rotating myosin clusters determine cytokinetic ring constriction. *Nat. Commun.* 7:11860.

30. Nixon-Abell, J., C. J. Obara, …, J. Lippincott-Schwartz. 2016. Increased spatiotemporal resolution reveals highly dynamic dense tubular matrices in the peripheral ER. *Science.* 354:aaf3928.

31. Toyota, T., D. A. Head, …, D. Mizuno. 2011. Non-Gaussian athermal fluctuations in active gels. *Soft Matter.* 7:3234–3239.

32. Park, Y., C. A. Best, …, M. S. Feld. 2010. Metabolic remodeling of the human red blood cell membrane. *Proc. Natl. Acad. Sci. USA.* 107:1289–1294.

33. Ben-Isaac, E., Y. Park, …, Y. Shokef. 2011. Effective temperature of red-blood-cell membrane fluctuations. *Phys. Rev. Lett.* 106:238103.

34. Trepat, X., M. R. Wasserman, …, J. J. Fredberg. 2009. Physical forces during collective cell migration. *Nat. Phys.* 5:426–430.

35. Bursac, P., G. Lenormand, …, J. J. Fredberg. 2005. Cytoskeletal remodelling and slow dynamics in the living cell. *Nat. Mater.* 4:557–561.

36. Fodor, É., M. Guo, …, F. van Wijland. 2015. Activity-driven fluctuations in living cells. *EPL.* 110:48005.

37. Farhadifar, R., J.-C. Röper, …, F. Jülicher. 2007. The influence of cell mechanics, cell-cell interactions, and proliferation on epithelial packing. *Curr. Biol.* 17:2095–2104.

38. Käfer, J., T. Hayashi, …, F. Graner. 2007. Cell adhesion and cortex contractility determine cell patterning in the Drosophila retina. *Proc. Natl. Acad. Sci. USA.* 104:18549–18554.

39. Bi, D., J. H. Lopez, …, M. L. Manning. 2015. A density-independent rigidity transition in biological tissues. *Nat. Phys.* 11:1074–1079.

40. Bi, D., X. Yang, …, M. L. Manning. 2016. Motility-driven glass and jamming transitions in biological tissues. *Phys. Rev. X.* 6:021011.

41. Bi, D., J. H. Lopez, …, M. L. Manning. 2014. Energy barriers and cell migration in densely packed tissues. *Soft Matter.* 10:1885–1890.

42. Forgacs, G., R. A. Foty, …, M. S. Steinberg. 1998. Viscoelastic properties of living embryonic tissues: a quantitative study. *Biophys. J.* 74:2227–2234.

43. Guevorkian, K., M.-J. Colbert, …, F. Brochard-Wyart. 2010. Aspiration of biological viscoelastic drops. *Phys. Rev. Lett.* 104:218101.

44. Stirbat, T. V., A. Mgharbel, …, H. Delanoë-Ayari. 2013. Fine tuning of tissues' viscosity and surface tension through contractility suggests a new role for α-catenin. *PLoS One.* 8:e52554.

45. Sekimoto, K., and S. Sasa. 1997. Complementarity relation for irreversible process derived from stochastic energetics. *J. Phys. Soc. Jpn.* 66:3326–3328.

46. Sekimoto, K. 1997. Kinetic characterization of heat bath and the energetics of thermal ratchet models. *J. Phys. Soc. Jpn.* 66:1234–1237.

47. Fodor, É., K. Kanazawa, …, F. van Wijland. 2014. Energetics of active fluctuations in living cells. *Phys. Rev. E Stat. Nonlin. Soft Matter Phys.* 90:042724.

48. Harris, A. R., L. Peter, …, G. T. Charras. 2012. Characterizing the mechanics of cultured cell monolayers. *Proc. Natl. Acad. Sci. USA.* 109:16449–16454.

49. Fodor, É., W. W. Ahmed, …, F. van Wijland. 2016. Nonequilibrium dissipation in living oocytes. *EPL.* 116:30008.

50. Harada, T., and S. Sasa. 2005. Equality connecting energy dissipation with a violation of the fluctuation-response relation. *Phys. Rev. Lett.* 95:130602.

51. Toyabe, S., T. Okamoto, …, E. Muneyuki. 2010. Nonequilibrium energetics of a single F1-ATPase molecule. *Phys. Rev. Lett.* 104:198103.